Ionofibers: Ionically Conductive Textile Fibers for Conformal i-Textiles

Claude Huniade,* Daniel Melling, Cédric Vancaeyzeele, Giao T.-M. Nguyen, Frédéric Vidal, Cédric Plesse, Edwin W. H. Jager, Tariq Bashir, and Nils-Krister Persson

With the rise of ion-based devices using soft ionic conductors, ionotronics show the importance of matching electronic and biological interfaces. Since textiles are conformal, an essential property for matching interfaces, light-weight and comfortable, they present as an ideal candidate for a new generation of ionotronics, i-textiles. As fibers are the building blocks of textiles, ionically conductive fibers, named ionofibers, are needed. However, ionofibers are not yet demonstrated to fulfill the fabric manufacturing requirements such as mechanical robustness and upscaled production. Considering that ionogels are known to be conformal films with high ionic conductivity, ionofibers are produced from commercial core yarns with specifically designed ionogel precursor solution via a continuous dip-coating process. These ionofibers are to be regarded as composites, which keep the morphology and improve the mechanical properties from the core yarns while adding the (ionic) conductive function. They keep their conductivity also after their integration into conformal fabrics; thus, an upscaled production is a likely outlook. The findings offer promising perspectives for i-textiles with enhanced textile properties and in-air electrochemical applications.

1. Introduction

Textiles are everywhere. We spend 99% of our lives in contact with textiles and due to this ever presence we tend to forget why

C. Huniade, T. Bashir, N.-K. Persson
The Swedish School of Textiles
Polymeric E-textiles
University of Borås
Borås 501 90, Sweden
E-mail: claude.huniade@hb.se

D. Melling, E. W. H. Jager
Sensor and Actuator Systems (SAS)
Department of Physics, Chemistry and Biology (IFM)
Linköping University
Linköping 581 83, Sweden

C. Vancaeyzeele, G. T.-M. Nguyen, F. Vidal, C. Plesse
Laboratoire de Physicochimie des Polymères et des Interfaces (LPPI)
Institut des Matériaux
CY Cergy Paris Université
Cergy-Pontoise Cedex 95031, France

The ORCID identification number(s) for the author(s) of this article can be found under https://doi.org/10.1002/admt.202101692.

textiles are so unique. Their properties are often summarized as light-weight, flexible, stretchable, comfortable, aesthetically pleasing, durable, and reusable.[1] All of these properties are the results of how conformal textile fibers and, ultimately, fabrics are.

By conformal, we mean the ability for an object to mold or shape dynamically after its handling; in other words and to a certain extent, we mean their geometrical adaptability. Conformality is an aim for wearable electronics, an aim beyond flexibility and stretchability.[2] This aim is especially relevant for e-textiles as there is a need of electroconductive fibers that can be processed into seamlessly integrated textiles, that is the deepest level of integration of fibers in textiles through fabric manufacturing processes like weaving and knitting.[3] The electronically conductive properties of these fibers are provided by the charge carriers of conductive materials that are commonly electrons and holes from metals or electroconductive plastics based on doped conductive polymers and electroconductive fillers such as metal particles or carbon allotropes.[4] As for today, conductive fibers can be stiff, brittle, difficult to process in fabrics and not durable enough as a product.[3,5] This is due to the inherent properties of the electronic conductive materials.[5,6] Therefore, it requires a laborious balance between desired properties to produce conformal e-textiles.

On the opposite, while living matter is soft, it also conducts electrical signals, and this conduction mostly involves ions as charge carriers. This observation is shifting the paradigm of electron-based devices to the rise of ion-based devices using soft ionic conductors.[7] We categorize all consistent substances in which ions are the predominant charge carriers as ionically conductive mediums or ICMs. Well-known examples of ICMs are electrolyte solutions, i.e., free ions dissolved in a polar solvent, or ionic liquids (ILs).[8] ILs are liquids comprised entirely of ions,[9] often with melting points lower than 100 °C, some even below room temperature. ILs have many advantages compared to electrolyte solutions, like higher thermal and electrochemical stability, as well as nonvolatility. Due to their undefined shape, liquid ICMs lack the self-standing ability which led to the development of quasi solid-state electrolytes and more specifically ionogels. Ionogels are ICMs where an IL is entrapped by a solid matrix such as a polymer network. In these systems,

the polymer network and the liquid are percolated throughout each other. The polymer network makes the gel an elastic solid while the liquid phase provides ions. Consequently, it forms a conformal ICM with good mechanical stability in combination to the main properties of the IL except outflow.[10]

Textile applications for ionogels are ionotronics: conformal energy storage devices, bioelectronic interfaces, photovoltaic devices, electroluminescent devices, textile sensors, and artificial muscles. Merging ICMs and textiles gives what we denote ionotronic textiles or i-textiles, in juxtaposition to electronic textiles or e-textiles containing electron- and hole-based conductive components. However, the integration of ICMs in a fabric for conducting purposes by seamlessly integrating ionofibers has yet to be proven. Ionofibers could either be produced directly into a filament form from an ICM, what we call bulk ionofibers, or be the result of functionalization by coating pre-existing core textile filaments, surface ionofibers.

Previous studies have attempted to produce ionofibers,[11–15] in which the fiber form-factor is used for its high surface-to-volume ratio and high aspect ratio (length-to-diameter ratio).[16] Indeed, for electroluminescent devices, the junctions[13] or interlacings[14] are key to the function through the contact points at the surface of the fibers. For sensing and actuating purposes, the surface is the most sensitive and responsive part of the fiber due to being first to experience stimuli.[15] Most of these attempts have another point in common: they focused on bulk ionofibers. Mechanically, ICMs are rather weak and soft which is why, in the form of bulk ionofibers, they have not seen much attention regarding their textile processability. Only one of those attempted bulk ionofibers presented a seamlessly integrated i-textile but without focus on the textile processability of their ionofiber.[14]

During fabric manufacturing processes like knitting or weaving, ionofibers can be exposed to temperature and humidity changes, to volatile particles in the form of dust or fibrils and also to mechanical forces. These mechanical forces are the most constraining phenomenon that can either make or break a fabric. They are due to the many contacts fibers have with different components in the many steps of construction. Friction causes the fibers to be twisted, tensioned, stretched as well as sheared into patterns. Many parameters can hence be changed to accommodate to specific needs and fibers. But, to summarize, a sufficient level of tenacity and friction is required for the fabric manufacturing processes. Thus, ionofibers are required to be processable in fabric manufacturing processes and to keep a certain level of their ionic conductivity in their integrated state. To achieve these requirements, an alternative solution to bulk ionofibers is surface ionofibers. Ionogel coated textiles have already been reported twice and both show mechanical robustness in the form of an ionogel-coated carbon nanotube yarn and an ionically conductive ionogel-coated silk fabric.[12,17] However, surface ionofibers have yet to be developed broadly for fabric manufacturing processes.

Therefore, we propose surface ionofibers that combines the excellent mechanical properties of commercial core yarns with the functional properties of an ionogel. This kind of ionofiber can address its function while keeping its textile properties and its fiber form-factor thanks to the conformality of ionogels, enabling a seamless integration in i-textiles. Our study focuses on the coatability of an ionogel as an in situ polymerized layer onto core yarns via dip-coating and on the effects of the ionogel coating on the characteristics of these ionofibers. The characterization comprises tensiometry, coating uptake analysis, lengthwise and cross-sectional optical microscopy, tensile testing, dynamical mechanical thermal analysis (DMTA), and electrical impedance spectroscopy (EIS). The textile processability of the ionofibers is assessed through a degradation analysis after two different fabric manufacturing processes, knitting and weaving. Knitted samples will be used to show the conformality and the usability of the ionofibers after a seamless integration into an i-textile with an application example as a movement and pressure sensor.

2. Results and Discussion

2.1. Preparation of Ionofibers

As a prevalent approach for functionalizing textiles, dip coating is a straightforward method and does not require specialized or expensive equipment.[18] We chose dip coating to form ionofibers since it has a long history related to textile dyeing and can be upscaled for continuous production. A long, continuous length of yarn has to be used in order to be manufactured into fabrics. We chose viscose and polyamide 6/6 as substrate for the coating of ionogels since they represent two categories of textile fibers: cellulose fibers and synthetic fibers. Also, they can be found commercially in the form of multifilament yarns. Filaments are continuous fibers and allow functional properties to be tailor-made for a particular end use.[19] In our case, multifilaments were interesting for their higher regularity and less complex structure when compared to staple yarns. Unfortunately, textile fibers do not have well-defined cross-sections. They have irregular and uneven cross-sections with noncircular shapes along their length. But the most confusing feature in regard to their cross-section is the space between the fibers of a yarn. Thus, it can be inconsistent to use a diameter to describe the fiber size. Instead in the textile industry, their linear mass density (i.e., mass per unit length), also known as fiber fineness, is conveniently used and gives consistent information from the molecular to the macroscopic level.[20] The fiber fineness is usually expressed in decitex or dtex. A tex is defined as 1 g km^{-1} or 10^{-6} kg m^{-1} in SI units, so a dtex equals to 10^{-7} kg m^{-1}.

The core yarns investigated were nontexturized multifilaments with viscose (dtex 167/44/1) and DuPont's Tactel strata as polyamide 6/6 (dtex 156/71/1), abbreviated Visc and PA, respectively. The dimensions of multifilaments are given with three numbers: the first number corresponds to the fineness of a ply of the yarn, the second to the number of filaments of the ply, and the third to the number of plies. Theoretically, these two core yarns have similar "diameters" of roughly 140 µm when assuming an optimal packing of circular filaments and their mass densities (1520 kg m^{-3} for Visc and 1140 kg m^{-3} for PA).

The ionogel synthesis was inspired from the work of Zhong et al.[21] In our case, EMIm OTf has been chosen astutely as ionic liquid and as base catalyst, which allows getting rid of adding chemicals and photoactivation of the polyaddition.

Table 1. Composition of the different samples. The weight ratio wt% of ILsoln is in regard to the total mass of the ionogel precursor and not the mass of the ionofiber.

Abbreviation	Ionogel recipe	Functional groups molar ratio			ILsoln [wt%]	Core yarn
		Thiol "TT"	Thiol "DT"	Acrylate "DA"		
TT25	(TT25DT75|DA90)ILsoln50	0.25	0.75	0.9	50	–[a]
TT100	(TT100|DA75)ILsoln50	1	–	0.75	50	–[a]
Visc-TT25	(TT25DT75|DA90)ILsoln50	0.25	0.75	0.9	50	Viscose
Visc-TT100	(TT100|DA75)ILsoln50	1	–	0.75	50	Viscose
PA-TT25	(TT25DT75|DA90)ILsoln50	0.25	0.75	0.9	50	Polyamide 6/6
PA-TT100	(TT100|DA75)ILsoln50	1	–	0.75	50	Polyamide 6/6

[a]Ionogel only.

In this case, acetic acid has been used a stabilizing agent to inhibit the polymerization in stock solution. The chemicals used to form the ionogels were: trimethylolpropane tris(3-mercaptopropionate) (TT); 1,4-butanediol bis(thioglycolate) (DT); poly(ethylene glycol) diacrylate (DA); an ionic liquid solution (ILsoln) made from 1-ethyl-3-methylimidazolium trifluoromethanesulfonate (EMIm OTf) and acetic acid (AcOH) (Table S1 and Figure S1, Supporting Information). The gel was formed through thiol–acrylate Michael addition reaction (also known as thiol–ene reaction) with TT and DT providing the thiol groups, DA providing the alkene groups, and the ionic liquid EMIm OTf acting as a base catalyst. In this work, two compositions of ionogel have been studied, as shown in **Table 1**, with nonstoichiometric ratios between the functional groups (more thiol than acrylate) and differentiated by the amount of trifunctional thiol (TT). ILsoln always represented 50% of the final ionogel mass. The (TT25DT75|DA90)ILsoln50 recipe, abbreviated TT25 here, included the chain extender DT which resulted in a lower cross-link density than (TT100|DA75)ILsoln50, abbreviated TT100 (**Figure 1**). TT25 presumably formed a softer and more conductive ionogel than TT100. These selected ionogels are based on our previous work that combined ILs with low viscosity photocurable precursors of the thiol–ene network

to synthesize patternable organic ionogel films with tunable mechanical properties.[21] There, a weak catalytic effect of the IL (EMIm TFSI) was noticed for the curing reaction which was designed to be initiated through a base catalyst or a photobase generator for the preparation of ionogel films. In this paper, we have used further this catalytic effect by choosing astutely to work with an already basic IL (EMIm OTf) as a substitute to a photobase generator for the curing of the ionogel (see experimental details in the Supporting Information). A volatile acidic solvent (AcOH) has been added to the precursor mixture as a stabilizing agent which can be evaporated naturally during the coating, leaving a basic medium in the mixture and initiating the polyaddition.

As the volume of ionogel precursor to be coated was exiguous, a small-sized bath was constructed to restrain most of the precursor's volume around the fiber. A cross-slit cap was fixed to the rim of the bath in order to withdraw the excess of material taken with the upward motion of the fiber (Figure 1). The fibers were drawn at a constant speed of 2.011 m min⁻¹ by an in-house built motor attaining up to 2-m-long samples. To allow them to cure, the samples were maintained vertically in ambient air for at least 2 days for precautionary measures. Prior to their characterization, the fibers were kept stored in a
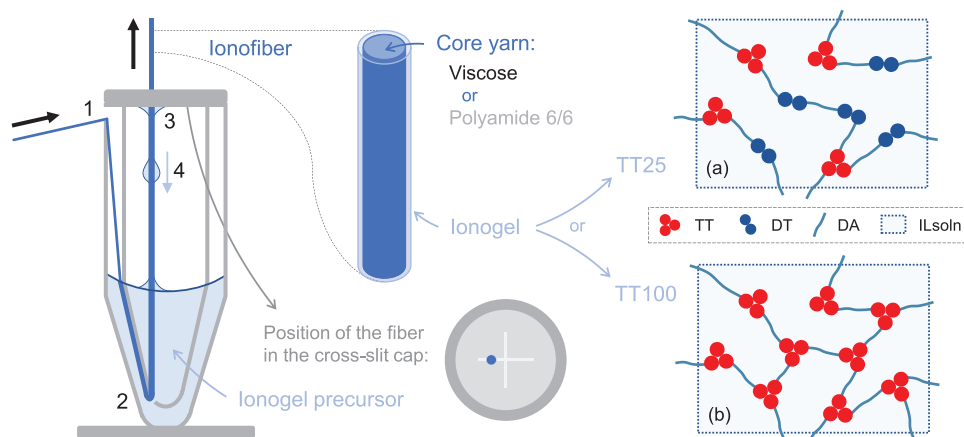

Figure 1. Dip-coating setup and composition of the ionofiber. Left side: schema of the low-volume bath with the fiber and the cross-slit cap. The fiber starts passing through (1) a V-shaped cut to enter the outer tube, then (2) a hole in the inner tube, and finally (3) the cap that helps to push the precursor between the filaments while also removing excesses. The excesses form eventually (4) a droplet that falls back to the bath. Right side: idealized network schematics for thiol acrylate formulation with excess thiol groups of (a) TT25 with DT as chain extender and (b) TT100 without DT.
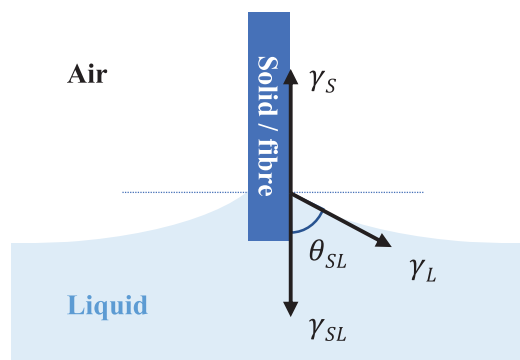
Figure 2. Contact angle measurement of an ideal fiber and Young's equation[22] quantities: θ_{SL} – contact angle of liquid on solid surface, γ_S – surface energy of the solid, γ_L – surface tension of the liquid, γ_{SL} – interfacial tension at solid–liquid interface.

conditioned atmosphere of 21 °C and 65% RH (percent relative humidity). Since both recipes were applied on both Visc and PA, there was a total of 4 combinations of ionogel and core yarn, namely, Visc-TT25, Visc-TT100, PA-TT25, and PA-TT100 (Table 1).

2.2. Coatability of Ionogels

The coatability of the ionogels was assessed through two complementary methods. First, the tensiometry measuring the material interfacial tension between liquid, solid, and gas phases was done through the optical observation of the different interfaces. Second, a practical approach was applied through measurements of the coating uptake and the visual observation of the ionofibers via an optical microscope.

An extensive literature is available about the theories behind the approximation of interfacial tensions. The theories are mainly based on Young's equation,[22] Dupré's expression for the work of adhesion,[23] and Young–Laplace–Gauss's equation.[24] Here, we focused on Fowkes theory to reach a sufficient level of approximation for the amount of experimental work needed,[25,26] from which we developed an adapted method to take into account the uneven surface of textile fibers (Equations (S1)–(S8), Supporting Information). Our method relies on the

menisci formed by the contact of the fibers with the liquids, as shown in **Figure 2**.

Tensiometry results are presented in **Table 2** (contact angles and supplementary results available in Table S2, Supporting Information). The surface tension γ_L of TT100- and TT25-precursors were similar, 42.20 and 42.35 mN m^{-1}, respectively, which translates as a close to identical time to reach their surface equilibrium. In comparison with an example in the literature, waterborne acrylic coatings have similar γ_L in the range of 45 mN m^{-1}.[27] The surface energies γ_S of Visc and PA, 76.27 and 73.21 mN m^{-1}, respectively, were relatively high compared to the example of solid plastic substrates with 20 to 50 mN m^{-1}. This implies a good attraction by the core yarns. In combination with the γ_S of the core yarns being higher than the γ_L of the precursors, the precursors show a good adhesion to the surface of the core yarns. In general, the higher the surface tension of the solid γ_S relative to the surface tension of the liquid γ_L, the better the wettability will be on the yarn by the liquid.[27] The nuances of γ_S between Visc and PA were minor but leaning toward a better wetting on Visc due to a higher γ_S. With the lower interfacial tension γ_{SL} of TT100 compared to TT25, TT100 would be slightly but not substantially easier to coat than TT25. With a larger disparity of γ_{SL} between TT100 and TT25 with PA (37.64 vs 40.01 mN m^{-1}) than with Visc (34.66 vs 40.76 mN m^{-1}), a difference due to the choice of the precursor should be slightly more noticeable when coating on PA.

The coating of ionogel resulted in increases of the fineness for the ionofibers from 167 dtex to between 235 and 256 dtex with Visc and from 156 dtex to between 200 and 230 dtex with PA as core yarns. The coating uptake (Equation (S9), Supporting Information) showed the regularity on the coating process with margins of error ranging from 0.8% to 3.0% with 90% confidence interval (CI) (**Figure 3**). Note that for some combinations, only a few samples were produced which explains the seemingly higher margins of error. With a higher increase in fineness when using Visc as core yarn (an average of 78 dtex vs 52 dtex when using PA), this clear trend confirmed the dependence of the core yarn on the amount of ionogel coated. When comparing the coating uptakes, this same trend was mitigated due to the difference of fineness of the core yarns but was still present.

These results from tensiometry and the coating uptake were mostly coherent. Indeed, the ionogel precursors adhered well

Table 2. Tensiometry results of the different combinations of core yarn and ionogel precursor. Results are presented as mean values ±95% confidence interval (CI). γ_S and γ_{SL} values are calculated from γ_L and contact angles (θ_{SL}). Sample size (n) for γ_L of TT25 = 121, for γ_L of TT100 = 185 and for each θ_{SL} used = 16.

Core yarn	Ionogel precursor	γ_L[a] [mN m^{-1}]	γ_S[a] [mN m^{-1}]		γ_{SL} [mN m^{-1}]	
Visc	TT25	42.20 ± 0.00026	76.27	+2.16	40.01	+3.08
				−2.65		−3.07
Visc	TT100	42.35 ± 0.00498	76.27	+2.16	37.64	+2.61
				−2.65		−2.56
PA	TT25	42.20 ± 0.00026	73.21	+3.60	40.76	+1.74
				−4.44		−2.41
PA	TT100	42.35 ± 0.00498	73.21	+3.60	34.66	+3.75
				−4.44		−3.41

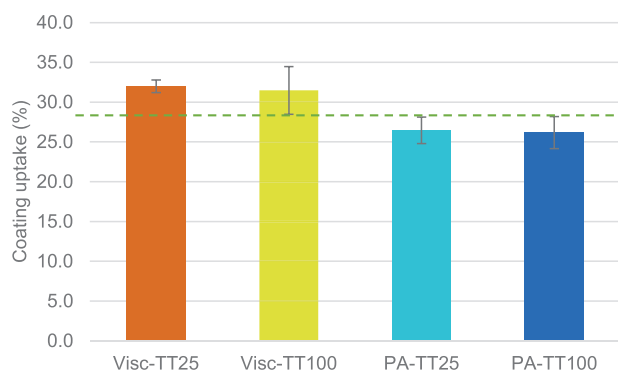[a]Independent of the core yarn (for γ_L) or the precursor (for γ_S).

Figure 3. Coating uptakes of the different combinations of ionofibers. Results are presented as mean values ±90% CI. Sample sizes (*n*) are 20, 3, 12, and 3 for Visc-TT25, Visc-TT100, PA-TT25, and PA-TT100, respectively. The green dashed line exposes the difference of uptake between Visc and PA.

to the surface of both core yarns averaging around 29% of the total mass of the ionofibers after curing. A slightly higher coating uptake for Visc (by 5.4% points) was present as expected from the analysis of the surface tensions. This tendency is in accordance with the fact that EMIm OTf, the IL that amounts for almost 50% wt of the ionogel precursors, has good affinity with cellulose-based materials,[28] such as Visc. A discrepancy with the tensiometry results was found as no difference of coating uptake could be noticed between the formulations, even between PA-TT25 and PA-TT100. This shows the limited effect on the coating uptake of a change of the polymer network formulation. In comparison, the affinity of the IL with the core yarns had a noticeable effect.

The formation of the polymer network (i.e., curing) was verified through the measurement of the extractible content of separately made ionogel films. As soon as 24 h after leaving the films for curing, their extractible content already reached a maximum of 50% meaning the cross-linking of the polymer

network completed during that period of time. Regarding stability over time, the ionofibers have shown they remained stable even a year after coating.

2.3. Fiber Morphology

2.3.1. Lengthwise

In earlier attempts to coat the fiber with the ionogels, excessively coated fibers were obtained and showed different surfaces depending on the core yarn used (**Figure 4**). In the case of PA, the surface looked regular and straight (Figure 4a), whereas the Visc samples showed roughness as displayed by the light reflection in Figure 4b. These observations exhibit again the difference in the ionogel behavior depending on the core yarn used, as mentioned in Section 2.2. Additionally, we observed the formation of beads due to the Plateau–Rayleigh instability (Figure 4c).[29] Generally, liquid-based coatings appear as uniformly spaced beads when the film is formed slower than the instability. The instability is highly dependent on the fiber fineness and the coating uptake and partly dependent on the viscosity and the surface tension of the liquid.

By lowering the take-up speed with an in-house built motor and by adding a cross-slit cap for squeezing any excess of precursor, the formation of beads was prevented. These adjustments effectively reduced the coating uptake and resulted in a uniform coating as seen in **Figure 5**. The resulting surfaces were less prominent than previously seen in Figure 4. Microbeads were still apparent for PA-samples only, but at the filament level due to their minuscule size. The ionogel with lower cross-link density, TT25, formed much smaller microbeads, which was also observed for the beads of the excessively coated fibers. For samples made from Visc, no microbeads were visible due to the wettability and the stronger affinity of the IL on Visc. Overall, the surface of the fibers remained mesoscopically fibrous after the coating.
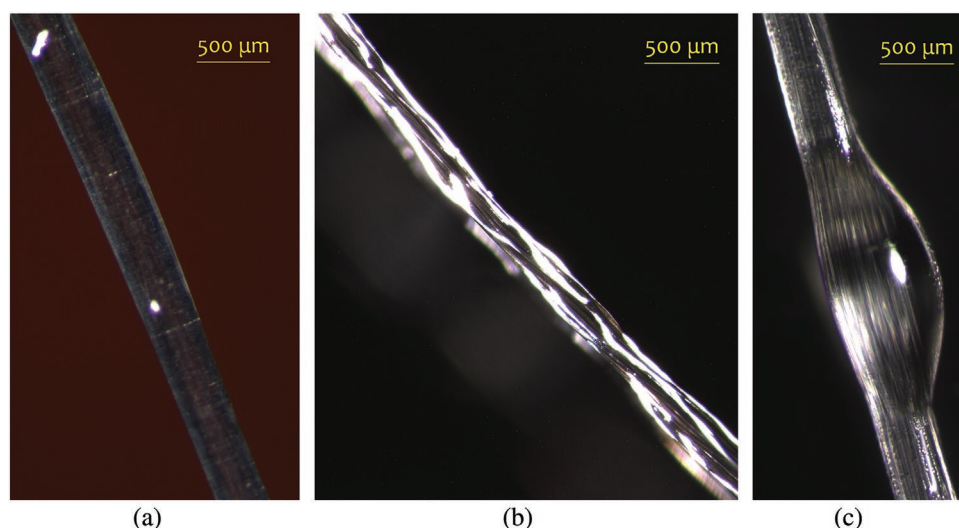

Figure 4. Observation of the excessively coated fibers. From left to right. a) Smooth surface when coating on PA. b) Rough surface when coating on Visc. c) Presence of beads.
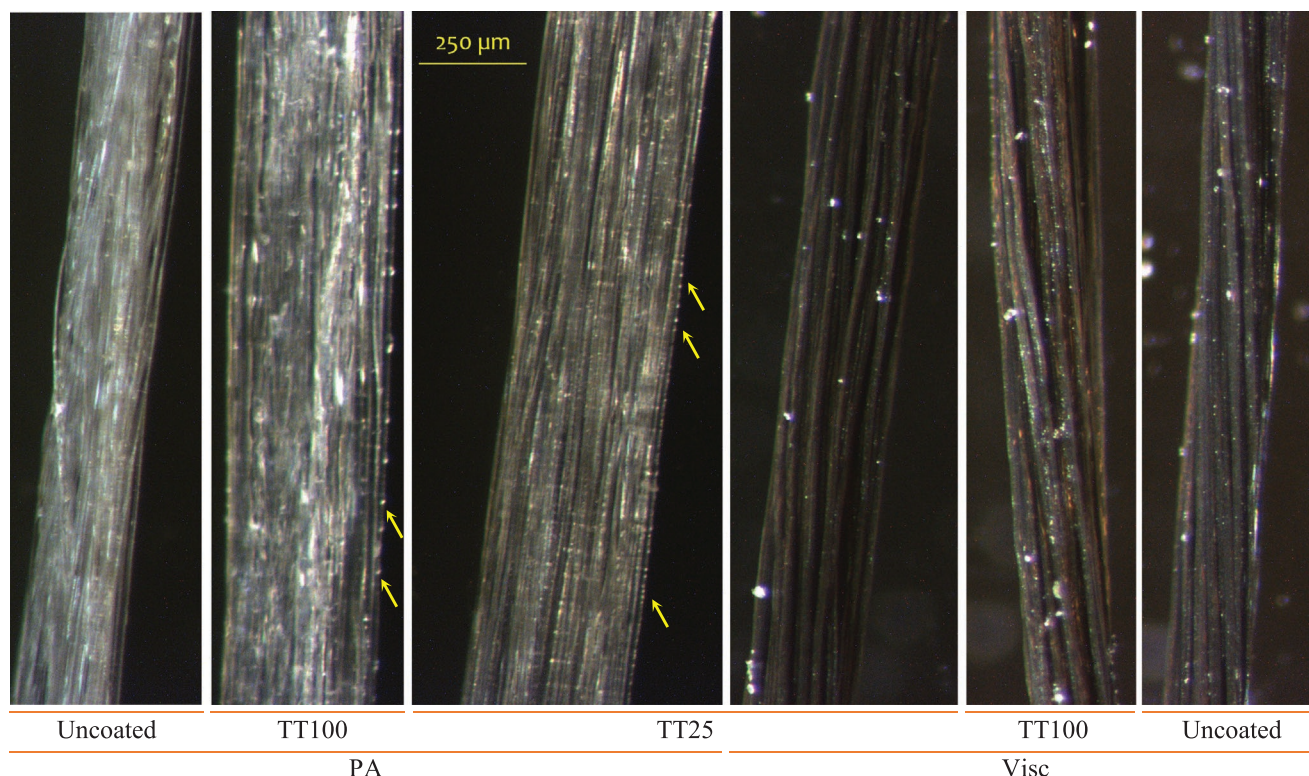
Figure 5. Lengthwise microscopy of the core yarns and the ionofibers. Every picture shares the same scale. The arrows show the position of a few microbeads. The microbeads can be easily differentiated from dust particles due to their relative uniform spacing.

2.3.2. Cross-Section

In **Figure 6**, the cross-sections of the ionofibers showed that the ionogel precursor managed to penetrate between the filaments to then form the ionogel which connected the filaments. The interfilaments pores were not completely filled as the biggest pores showed open areas. With the ionogel being formed around and within the yarn, this explains the unification of the filaments by the ionogel, now acting like a protective layer preventing easy delamination. The shape of the polyamide filaments seemed to not be influenced after coating although it is something difficult to assert. Indeed, despite their circular and trilobal shapes, the uncoated polyamide filaments show small irregularities just like the coated ones (Figure 6a,b). However, the viscose filaments with their cloud shape seemed to have been smoothened or even fused by the coating (Figure 6c,d). This effect can be attributed to the affinity of the IL with Visc and the smooth surface that ionogels produce when cured. In retrospect, the choice of a black-colored yarn was of poor decision regarding the optical observation since it is difficult to get a proper view of the ionogel, as the latter is transparent.

2.4. Mechanical Properties

To compare the elastic properties and ultimate strength of the ionofibers against the core yarns, the force–strain curves obtained by tensile testing are presented in **Figure 7**. Due to the morphology of PA, a two-step break was noticed. Since the morphology of PA, a two-step break was noticed. Since

the cross-sectional shape has an effect on the orientation of amorphous regions when the fiber is drawn, trilobal filaments tend to have a lower uniform strain than round filaments.[30] Therefore, the trilobal filaments in PA broke first at an average strain of 55% while the round ones broke at a higher average strain of 63%. This specific two-step break was not present for the ionofibers as the ionogel acted like a matrix forming a composite at the mesoscopic/yarn level. Additionally, different behaviors at rupture were observed. Indeed, after rupture, the core yarns had tapered broken ends whereas the ionofibers had rather sharp broken ends due to the filaments being unified by the ionogel. Since sharper ruptures are usually indicative of stronger fiber-to-fiber cohesion, these observations support the hypothesis of their strong interactions and the penetration of ionogel coating between the filaments of the core yarns. Since TT25 is a softer and more stretchable ionogel than TT100, we expected to see a clear distinction between the curves of the combinations of ionofibers made from the same core yarn. However, this distinction was absent. Yet, the force–strain curves clearly showed a difference in mechanical behavior between the ionofibers and their core yarns. Hence, we suspected that a combination of chemical and physical interactions between the ionogel and the core yarns were responsible for the aforementioned effects. These interactions can be due to the polymer network of the gel forming onto/into the surface of the filaments as well as their penetration into/between the filaments.

An extensive analysis was made using the initial slope, the maximal force, the tenacity, and the uniform strain, all
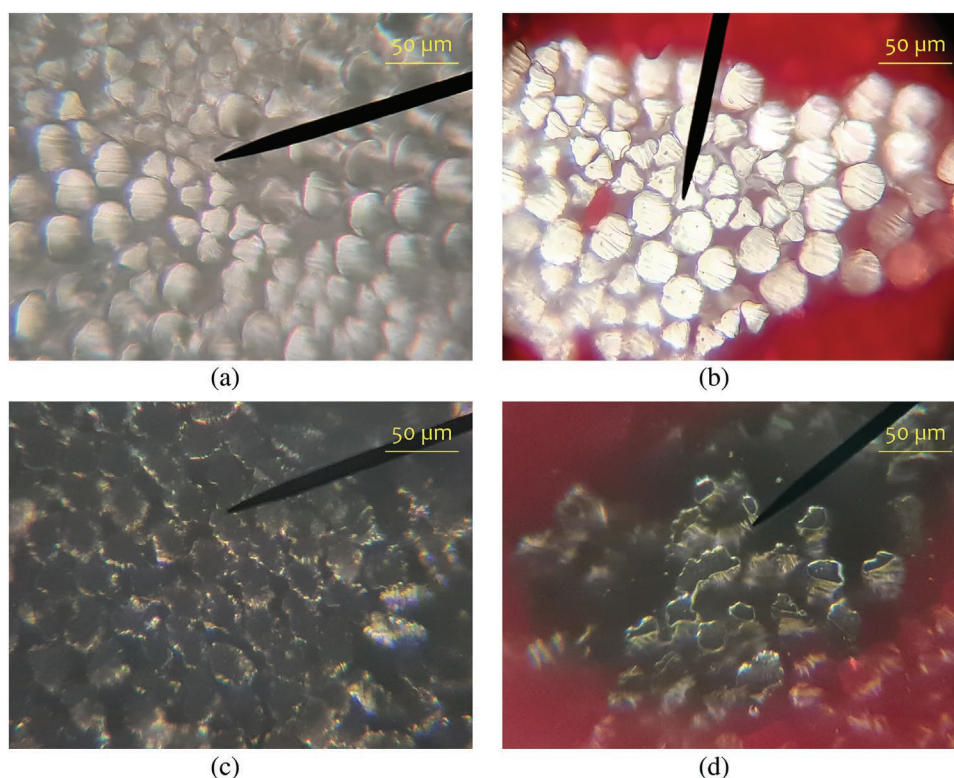
**ADVANCED
SCIENCE NEWS**
www.advancedsciencenews.com

**ADVANCED
MATERIALS
TECHNOLOGIES**
www.advmattechnol.de

Figure 6. Cross-sectional pictures of a) PA, b) PA-TT25, c) Visc, and d) Visc-TT25. The red background is polyester filaments used as filler for the preparation of the cross-section cuts (more details on the preparation in the Supporting Information).

extracted from the tensile tests (**Figure 8**). The linear part at low deformation represents the elastic part of the deformation from which the initial slope is extracted to quantify the stiffness of the material. The maximal force is the highest force reached during a test, whereas the tenacity specifically quantifies the force by the fiber fineness. Tenacity, also called specific strength, is used for textile fibers and is commonly expressed in cN tex^{-1}, equivalent to 10^4 Pa m^3 kg^{-1} or 10^4 N m kg^{-1} in SI units (tenacity–strain curves in Figure S2, Supporting Information). The uniform strain is defined as the strain at maximal force. First, the reduction of initial slope after coating indicates

Figure 7. Force–strain curves for core yarns and ionofibers. Sample sizes (*n*) are 5 for core yarns and 3 for ionofibers, with each line representing a single test. In order to exclude the added mass due to the coating from the analysis, force was used instead of tenacity.

the loss of stiffness, by 23% and 43% from the stiffness of Visc and PA, respectively. As the maximal force was not considerably influenced, the decrease of the tenacity after coating was prompted by the increase of the fiber fineness. The uniform strain of the ionofibers increased substantially by 66% and 50% compared to the uniform strain of Visc and PA, respectively. This extensive analysis indicates that the coating rendered the ionofibers more flexible than their core yarn, i.e., the ionogel seemingly has a plasticizing effect on the core yarn.

To prove the plasticizing effect of the ionogel, the viscoelastic properties of the ionofibers, the core yarns and the ionogel films were studied through DMTA in tensile mode by comparing the storage modulus E' and loss factor $\tan \delta$. Once again, due to working with the tenacity rather than the stress, the moduli were expressed here in N tex^{-1}. DMTA curves are presented in **Figure 9**. At low temperature, around -40 °C, the principal mechanical relaxations of the ionogel TT100, associated to its glass transition temperature T_g, was noticed through the onset of its storage moduli as well as the peaks of its $\tan \delta$ of TT100. Regarding TT25, its T_g seemed to be lower than -50 °C. On the ionofibers, the T_g of TT100 was clearly visible on PA but surprisingly not on Visc. Above 50 °C, a shift of the mechanical relaxation of PA to lower temperature was noticed, by 14 °C for the $\tan \delta$ peaks. Regarding Visc, since its T_g was close to its degradation temperature (280 °C), it is difficult to get the actual peak of its $\tan \delta$. Yet, both Visc-TT25 and Visc-TT100 have shown a clear $\tan \delta$ peak and shift of the T_g by more than 70 °C toward lower temperature. Thus, we have proof that the core yarns were plasticized by the ionogels in varying degree
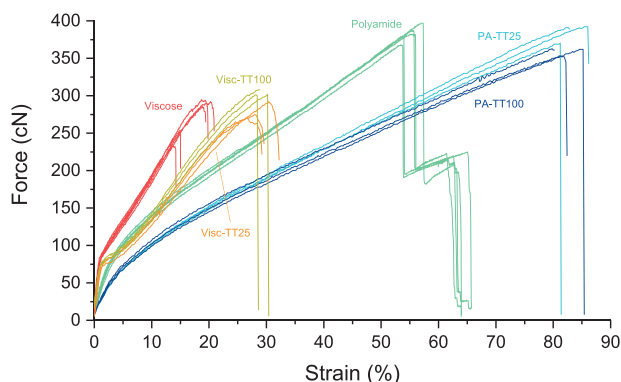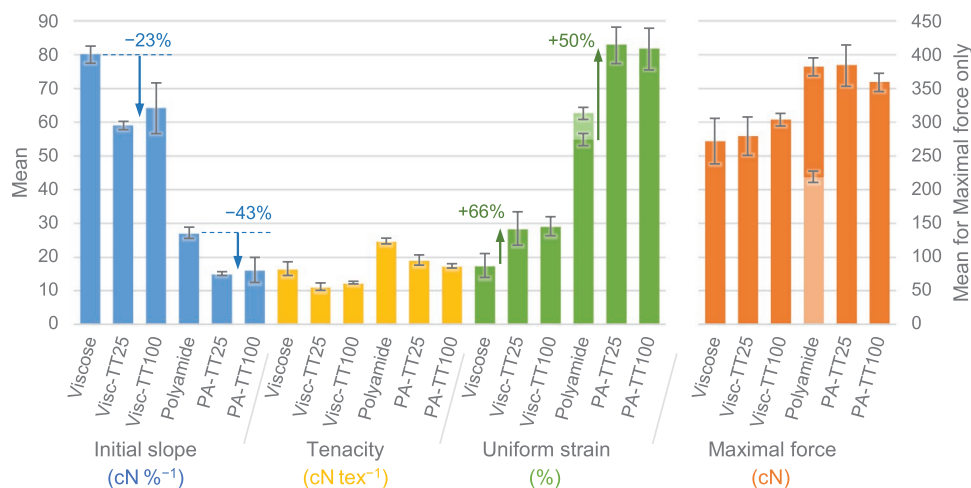
ADVANCED
SCIENCE NEWS
www.advancedsciencenews.com

ADVANCED
MATERIALS
TECHNOLOGIES
www.advmattechnol.de

Figure 8. Comparison of the tensile properties of core yarns and ionofibers. Results are presented as mean values ±95% CI ($n = 5$ for core yarns and $n = 3$ for ionofibers). Every property except the maximal force shares the left Y-axis for their mean value. Uncoated polyamide (PA) fibers have two maximal forces and two uniform strains due to their two-step breaking.

depending on the core yarn. Due to the now proven plasticizing effect of the ionogels on the core yarns, the composite material that is the surface ionofiber became more flexible than its core yarn alone was. Nonetheless, the mechanical properties of the core yarn were mostly kept and not much of a difference was seen between the recipes.

2.5. Conductivity of the Ionofibers

With the apparent continuous unity attained by the ionogel around and within the ionofibers, it was expected that the ionofibers would have regular conductive paths along their length. Additionally, the interactions between the ionogels and the core yarns could influence how much of the conductivity of the ionogels would be transferred to the ionofibers. Therefore, EIS was used to analyze the responses of our ionofibers samples to alternative current (AC) stimulation and was conducted using a two-point probe (**Figure 10**) at ambient temperature and relative humidity. The cylinder parts of the electrodes were held parallel and horizontal with a 20 mm space between their axes. The fibers were looped once around each electrode and held down by attaching clips with a weight of 3.6 g each on both ends.

The Nyquist plots from the EIS are shown in **Figure 11**, from which the charge transfer resistance (R_{ct}) of the ionofibers were extracted by fitting the semicircular parts of the data (corresponding circuit model and Bode plots in Figures S3 and S4, Supporting Information). The ionofibers behaved differently depending on their core yarn, as smaller semicircles were obtained for the samples with PA ($R_{ct} = 199$ MΩ for PA-TT25 and $R_{ct} = 239$ MΩ for PA-TT100) than with Visc ($R_{ct} = 248$ MΩ for Visc-TT25 and $R_{ct} = 441$ MΩ for Visc-TT100). The higher resistance of samples with Visc as core yarn is a result of the larger effect from the interactions of the ionogel with Visc. Despite their bigger coating uptake, these ionofibers probably had part of the IL trapped within their viscose filaments which could have been caused by their stronger affinity.[28]

Nonetheless, ionofibers made with TT25 have clearly lower resistances than those made with TT100. This was presumed by the lower cross-linking density of the polymer network structure, which does not impede the movement of the ions as much and therefore allow easier transfer of charges. The extracted resistances were then used to calculate the conductivity of the ionofibers.

Conductivity is commonly expressed in S m^{-1} or S cm^{-1} using the following formula

$$\sigma = \frac{L}{R \times A} \tag{1}$$

where L is the length of the sample between electrodes in m or cm, R is the resistance of the sample in Ω, and A is the cross-section area in m^2 or cm^2. In practice, just like discussed in Section 2.1 with the diameter, it is more convenient for fibers to base a definition on mass per unit length than on area of cross-section. With the same logic as Morton and Hearle when they proposed the mass specific resistance,[20] we propose to use the mass specific conductance as a conductivity property based on the linear density. This analogous property that we call the fiber conductivity is equivalent to the conductivity from Equation (1) divided by the volumetric mass density of the sample.

The fiber conductivity of the samples therefore denoted by σ_f were calculated by

$$\sigma_f = \frac{L}{R \times \lambda_m} \tag{2}$$

where R is the resistance of the sample in MΩ, L is the length between the contacts of the sample with the two electrodes in mm or cm, λ_m is the fineness of the sample in tex or dtex. We chose these units for practical convenience and expressed σ_f in µS mm tex^{-1} or µS cm dtex^{-1}, equivalent to 10^{-3} and 10^{-1} S m^2 kg^{-1} in SI units, respectively. Since the typical density of solids and liquids is in the range of 10^3 kg m^{-3}, the fiber conductivity is directly comparable with the conductivity in S m^{-1}

**ADVANCED
SCIENCE NEWS**

www.advancedsciencenews.com

**ADVANCED
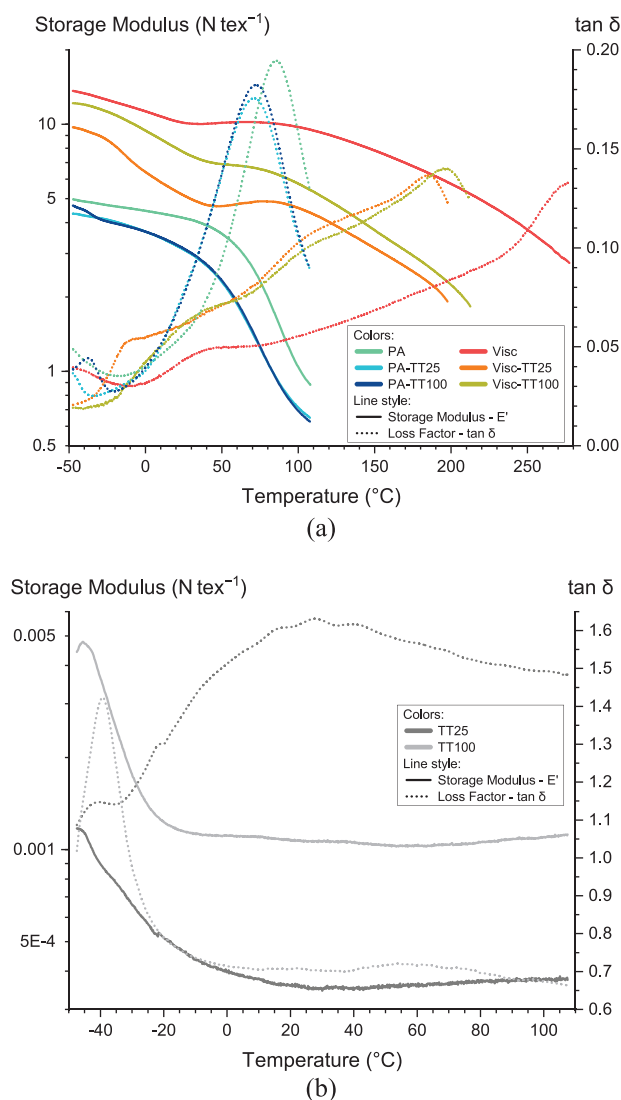MATERIALS
TECHNOLOGIES**

www.advmattechnol.de

Figure 9. DMTA curves of a) the ionofibers and the core yarns, and b) the ionogel films. Single measurements were done up to 110 °C for PA-based samples and ionogel films, and up to degradation for Visc-based samples.
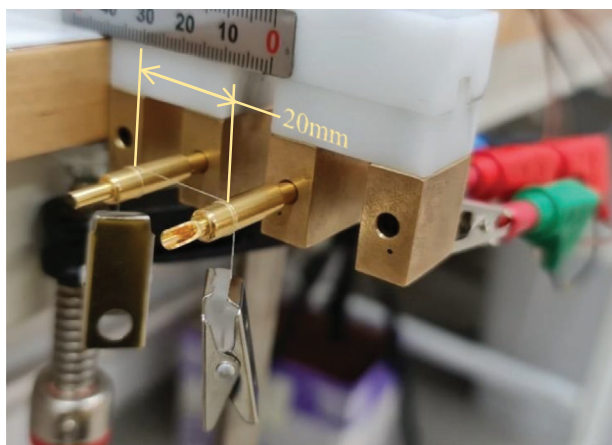

Figure 10. 2-point setup for the electroanalytical tests of the ionofibers, using gold-plated laboratory plugs as electrodes.
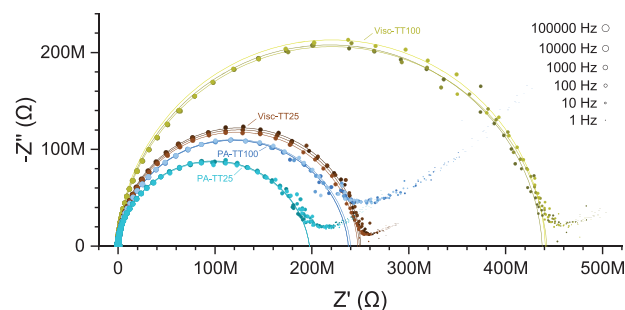

Figure 11. Nyquist plots of the EIS with the semicircular fittings ($n = 3$ per combination). Average ambient conditions: 21.6 °C and 12% RH.

or S cm^{-1}, respectively (more details about the formula and its unit in Figure S5, Supporting Information). Yet, the fiber conductivity is simpler to obtain and enables more scientifically sound comparisons not only between conductive fibers, but also with conductive films. Indeed, in order to evaluate the conductivity of a film versus the same film in the form of a fiber coating, a normalized fiber conductivity can be calculated by dividing the fiber conductivity σ_f with the coating uptake w_c. However, coatings can sometimes modify or fuse with the substrate which can make the normalized σ_f less accurate than the σ_f. Additionally, the orientation of the measurement is taken into account with σ_f which is especially relevant for textiles as they are known to be anisotropic.

The fiber conductivities calculated with Equation (2) are presented in **Figure 12**. The same trends were observed as mentioned in the previous paragraph. Measurements done several times without moving the samples showed that they were repeatable given the same ambient conditions. When measuring additional portions from the same fiber at different positions along the length, the resistances had a larger variation but remained similar. To accurately evaluate how much the core yarns can influence the conductivity of the coated ionogels, the fiber conductivity of a film from each ionogel formulation was measured for reference (**Figure 13**). Compared to the σ_f of the ionogel films (4.2×10^{-4} μS cm dtex^{-1} for TT25), the normalized σ_f of the ionofibers reached up to 2.1×10^{-4} μS cm dtex^{-1} for PA-TT25 which amounts to half of its counterpart. These decreases after coating are certainly an effect of interactions with the insulating core yarns. This comparison highlights the importance of characterizing with the non-normalized fiber conductivity as it is more representative of the ionofiber as a whole for the i-textile application. Nonetheless, this comparison demonstrates that, once coated on these core yarns, the ionogels kept their conductivity within an order of magnitude.

Due to their better conductivity, the combination of ionofibers with TT25 was selected for the supplemental measurements. First, the measurements were done by varying the distance between the electrodes (**Figure 14**). These measurements followed to a certain degree a linear regression through the origin with good R-squared values which enabled us to verify that contact resistances were negligible. In addition to the coating uptake results, they prove a certain level of uniformity along the length. Note that, in comparison with results shown in Figure 12, higher conductivities were obtained due to higher ambient relative humidity.
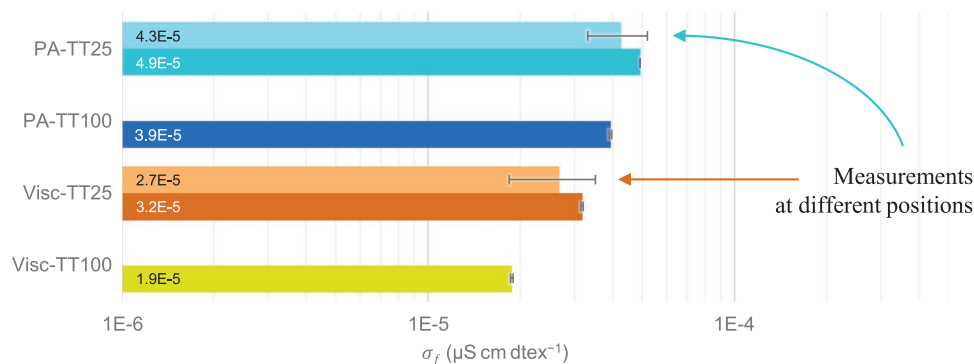
Figure 12. Fiber conductivity of different combinations of ionogel and core yarns. Results are presented as mean values ±90% CI, for $n = 3$. For the TT25 samples, measurements were also done along the length ($n = 5$, sampled from the same fiber).

All the previous results were measured on at least 3 months old samples, as they had already reached a stable level of fiber conductivity. Despite the quick curing and the stability of the ionofibers even a year after coating, a major drop of fiber conductivity was within the first weeks after coating. Therefore, an analysis of the fiber conductivity was performed over the first 60 days after coating (**Figure 15**). Two samples with each core yarn were used for this analysis, with the second sample being tested between 10 and 20 days after coating to get more data on the instability of fiber conductivity. This instability could be attributed to the ionic species within the ionofibers slowly reaching an equilibrium over time. The fiber conductivity was observed to stabilize after 20 days, but remained substantially influenced by the relative humidity as is the case for EMIm OTf.[31]

2.6. Influence of Fabric Manufacturing Processes on Functionality

The ionofibers have shown they could be stable even a year after coating. While being more flexible than their core yarn yet ionically conductive, the question remains whether they can withstand fabric manufacturing processes and keep their conductivity after their seamless integration. To answer this question, the textile processability of the ionofibers was investigated

through the knitting and weaving of basic structures by loading the ionofibers in a manual knitting machine and a digital handloom, respectively (see experimental details in the Supporting Information). Due to their higher fiber conductivity, we selected the ionofibers made with TT25 to construct fabrics with a conductive segment between segments of the corresponding core yarns. Two knitted samples were prepared for each core yarn, one including a single row of ionofiber as represented in **Figure 16**a, the other one a section with 15 rows of ionofiber. A single woven sample for each core yarn was prepared using a plain structure including a section made of six ionofibers in weft direction as represented in Figure 16b. The single row knitted sample was used to evaluate the effects of knitting on the conductivity of the fiber without having interconnections influencing the measurement. Whereas the 15 rows knitted sample was used for a broader evaluation of the processability of the ionofibers in knitting. Since thicker staple polyester yarns (Nm 40/2) were used as warps for the woven samples, no interconnections between the ionofibers could influence the evaluation of the conductivity.

2.6.1. Tacit Knowledge and Visual Evaluation of the Fabrics

Due to the length (around 90 cm) and fineness of the ionofibers (**Figure 17**), we were limited to prepare fabrics with a small
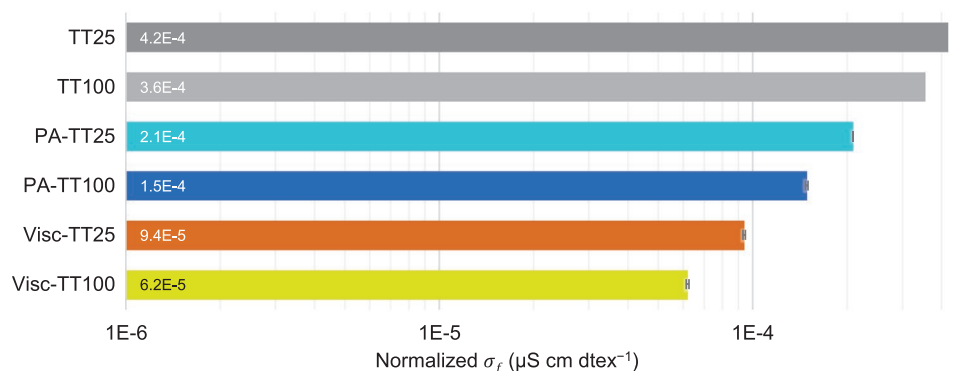

Figure 13. Comparison of the normalized fiber conductivities between the coated part of the ionofibers and the ionogel films. The normalized fiber conductivities were obtained by dividing the fiber conductivity with the coating uptake. The ionogel films TT25 and TT100 have a coating uptake of 1. Results are presented as single measured values for TT25 and TT100 ($n = 1$) and mean values ±90% CI for the ionofibers ($n = 3$).

**ADVANCED
SCIENCE NEWS**

www.advancedsciencenews.com

**ADVANCED
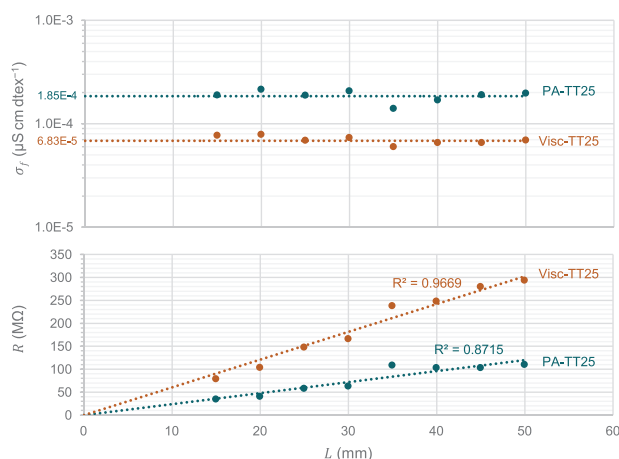MATERIALS
TECHNOLOGIES**

www.advmattechnol.de

Figure 14. Resistance and conductivity of the ionofibers made with TT25 in function of the length between the contact points. Results are presented as single measured/calculated values. The linear regression through the origin on the bottom graph shows that contact resistance is negligible. Average ambient conditions: 22.1 °C and 45% RH.

width and as dense as possible. Additionally, instead of feeding with the usual tension mast for knitting or the shuttle for weaving, the ionofibers were fed and tensioned manually, which could have resulted in uneven tension, but also a softer contact in terms of friction outside of the pattern making steps. Therefore, the assessment of the processability of the ionofibers in fabric manufacturing processes was done almost purely on a pattern making level at low speed. This assessment has its practical relevance in the fact that most of the damage is done at the pattern making level. The damage is a result of the abrasion, extension, and bending that the textile fibers are subject to when processed.

After folding an ionofiber on purpose and then illuminating it from above (Figure 17), the bended part of the ionofiber showed a different level of light reflection than its undamaged parts. This was due to microfractures in the polymer network of the ionogel, both on the surface and in between the filaments. This phenomenon was also observed when cutting or trying to delaminate the ionogel. This different level of light reflection
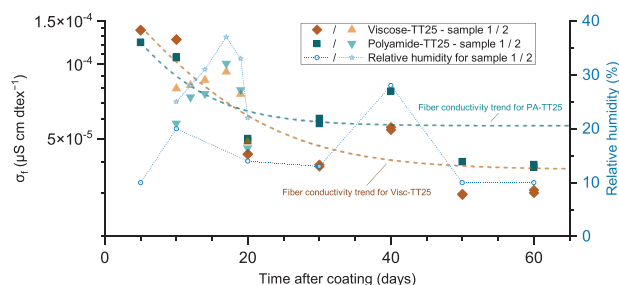

Figure 15. Fiber conductivities of ionofibers made with TT25 taken from EIS results over time after coating. Results are presented as single measured values ($n = 2$ for sample 1, $n = 1$ for sample 2). The fiber conductivity trends were obtained via exponential decay fittings of all the data points for a specific combination of ionogel and core yarn, without accounting for the relative humidity. Average ambient relative humidity is reported for each day of measurement.

was looked for on the fabric samples to evaluate the damage caused by the fabric manufacturing process to the ionofiber.

First, no breaks happened when knitting or weaving the ionofibers. Second, the ionofibers felt slightly smoother to knit or weave than the core yarns, mostly attributed to the antistatic effect of the ionogel coating. Third, as observed for the knitted fabrics in **Figure 18**, defects were due to the excess of manual tension, which also illustrates the difficulty of preparing a seemingly perfect knitted sample as textile is a very flexible material. No visual defect was detected on the woven fabrics. Due to the color of PA and the different light reflection by PA-TT25, the PA woven sample was the only sample with a clear distinction between the ionofibers and the core yarns.

The microscopic pictures of the knitted samples (**Figure 19**) barely showed a difference of light-reflection at the surface of the fibers due to damage. Whereas those of the woven samples did not show any damage (**Figure 20**). This also showed how difficult the differentiation between the woven ionofibers and core yarns turned out to be. As the polyamide filaments were slightly transparent, few microfractures of the ionogel coating were visible within the knitted ionofibers between the filaments. These microfractures resulted from the different levels of deformation the filaments were subjected to when the loops were formed. With these cumulative evidences of absence of degradation, we can assert that, to some degree, the ionogel acted as a protective coating layer for the core yarn.

2.6.2. Fiber Conductivity Stability

The main function of the ionofibers is directly related to their fiber conductivity σ_f. Thus, we developed a method to evaluate the degradation of the fiber conductivity caused by the fabric manufacturing processes. The ionofiber was required to be tested in three different states in order to get comparable results. The reason for the three states was that the fibers were crimped and pretensioned within the fabrics. Therefore, these three states were (see preparation details in the Supporting Information)

- in-fabric, the fiber was crimped and pretensioned by other fibers within the fabric,
- pulled-out, the fiber was simply taken out of the fabric and left with its crimp,
- stretched, the fiber was put on the 2-point setup for measuring σ_f (Figure 10).

A single reference result for both PA-TT25 and Visc-TT25 was taken from the previous ageing results. A more recent measurement for each of the reference sample was done to take into account the ambient conditions. Regarding the measuring setups, the crimped states shown in **Figure 21**, in-fabric and pulled-out, were directly comparable with each other. This was possible since the ionofiber was not removed from the clips in between the two states. By using the 2-point setup, the reference and stretched state were also comparable between themselves. However, these two comparisons were not sharing the same setup but were related by three facts.
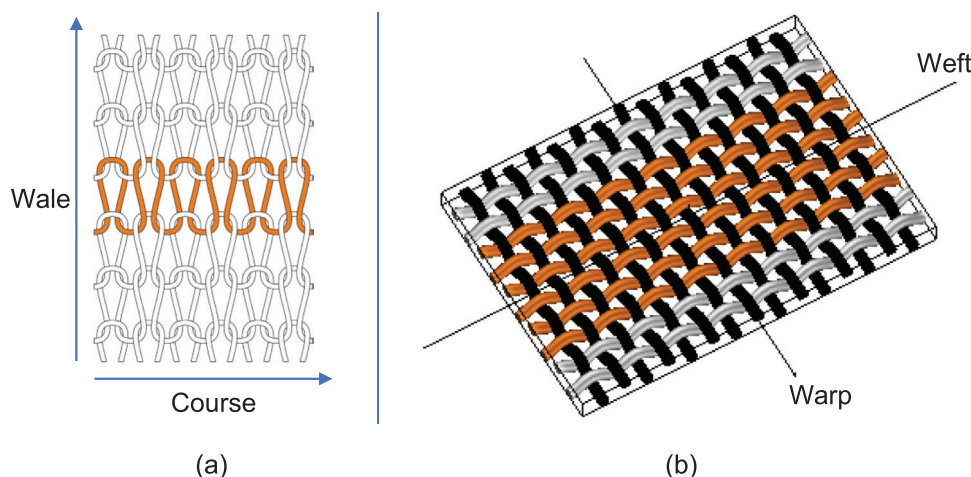
Figure 16. Schematic of the structure of the fabrics: a) 1 × 1 rib knitted fabric. b) Plain weave. Orange yarns represent ionofibers, white: core yarns, and black: polyester warps. The 15 rows knitted samples also used the same 1 × 1 rib structure but instead of a single row of ionofiber like represented, 15 rows of ionofibers composed the conductive segment.

- The same ionofiber sample was used for the three different states.
- The resistance of the ionofibers was proportional to their length.
- Ionofiber samples produced in different batches had similar fiber conductivities given the same ambient conditions of measurement.

Therefore, a comparison of the fiber conductivities was possible and is presented in **Figure 22**.

First and foremost, with a relative humidity of 46% RH, the conductivity of the reference ionofibers was higher than a previous measurement on the same sample at 10% RH. The conductivity of the reference ionofiber was measured for Visc-TT25 and PA-TT25 at 6.30×10^{-5} and $9.05 \times 10^{-5}\,\mu S\,cm\,dtex^{-1}$, respectively, versus the 3.87×10^{-5} and $3.05 \times 10^{-5}\,\mu S\,cm\,dtex^{-1}$ of the previous measurement at 10% RH. PA-TT25 remained more conductive than Visc-TT25, with a conductivity in-fabric of 1.82×10^{-4} versus $5.90 \times 10^{-5}\,\mu S\,cm\,dtex^{-1}$ for knitted ionofibers, and 2.14×10^{-4} versus $4.95 \times 10^{-5}\,\mu S\,cm\,dtex^{-1}$ for woven ionofibers. Once pulled-out, the conductivity of the woven ionofibers decreased slightly but relatively more for the knitted ones. A plausible explanation is that a slight change in the contact point or some damage happened when removing the ionofiber from the fabric, despite the careful handling. In the stretched state, woven ionofibers recovered

conductivities similar to the in-fabric state, whereas knitted fibers kept conductivities close to the pulled-out state. This difference supports the idea that, since a knitted ionofiber loops closely to itself, it could be in contact with itself. Therefore, a shorter connection would be made. In any case, all the conductivities measured were similar to the conductivity of the reference fibers after 101 days. Thus, these results support the previously mentioned evidences of absence of degradation.

Interconnections between the ionofibers were more prevalent on the 15 rows knitted samples. But this also meant a too complex structure to be able to properly calculate their conductivities. Consequently, their resistances per unit length of fabric (R/L) in each direction were used along with their mean in-fabric R/L to make a comparison of ratios, as presented in **Table 3**. The 15 rows samples have shown very different behavior depending on the core yarn. The ratio between the course direction R/L and the in-fabric R/L was three times bigger for PA-TT25 than for Visc-TT25. As PA was more flexible than Visc (cf. Section 2.4) and has a smoother surface (cf. Section 2.3.1), better interconnections were made in the PA-TT25 sample. This inference is supported by the R/L of the wale direction, which is purely based on an interconnection-basis due to the ionofibers being inserted in the course direction. Indeed, an even bigger difference was noticed depending on the core yarn: the ratio between the wale R/L and the course
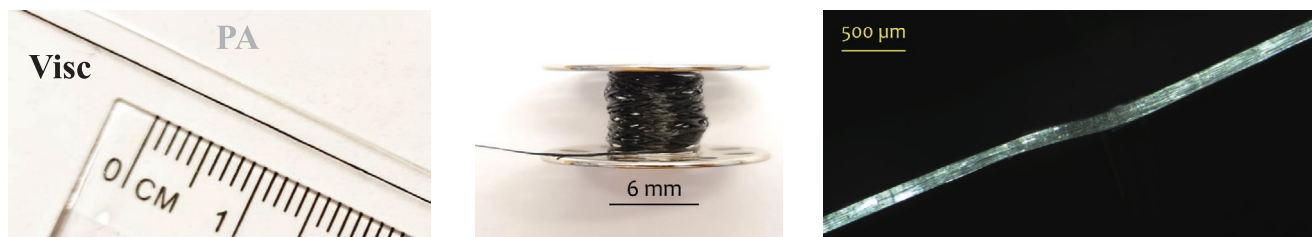

Figure 17. From left to right: core yarns next to a ruler, ionofiber on a spool, microscopic picture of an ionofiber showing lower reflection in its damaged part.
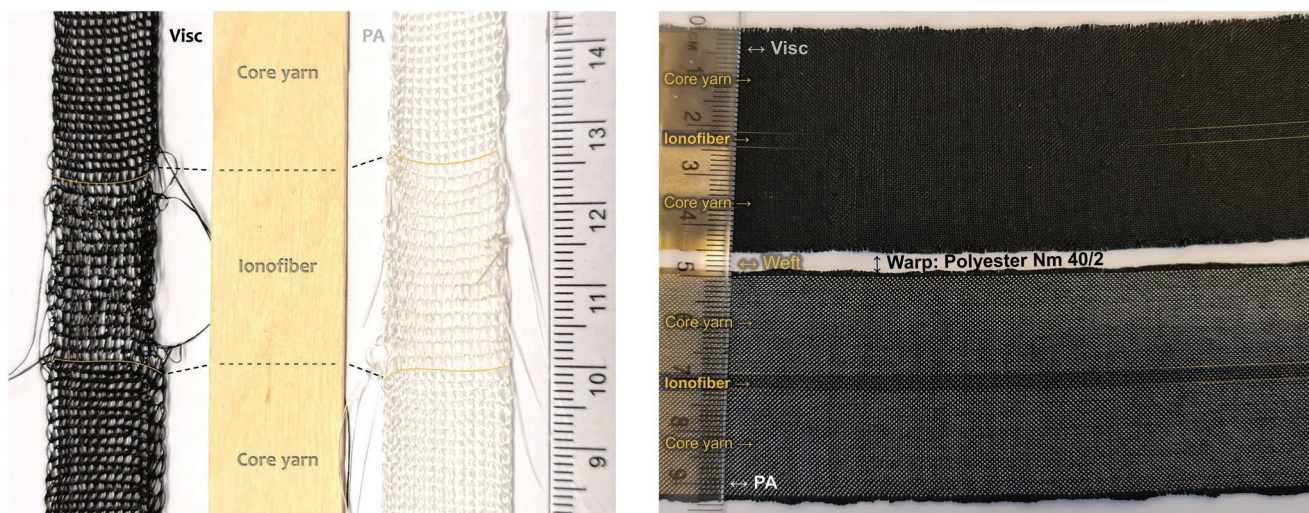
Figure 18. Left: knitted samples with an ionofiber section. Right: woven samples with an ionofiber section.

R/L for PA-TT25 was almost fivefold the ratio for Visc-TT25. The wale R/L being lower than the course R/L for both the samples can be attributed to the structure, since the fibers are more densely oriented in the wale direction.

In order to show how much the ionogel coating makes the fiber and therefore the fabric conform, we elaborated a comparison between knitted samples made with ionofibers versus ones made of core yarns only. Where flexible means bendable without breaking and stretchable additionally means able to sustain elongation, conformal adds the ability to deform under its own weight to adjust its shape. To assess the conformality of the fabrics, a simple test has been performed by dropping the samples from a small height onto a ⌀1.4 mm glass cylinder, the tip of a pipette (Movies (S1)–(S4), Supporting Information). The curvature of the samples was compared from the view normal to the glass cylinder axis. As illustrated in **Figure 23**, the ionofiber samples show a smaller curvature than their core yarn counterpart which proves an enhanced conformality. With a greater difference between their curvature, the PA samples clearly showed that ionofibers produce more conformal fabrics than uncoated fibers do.
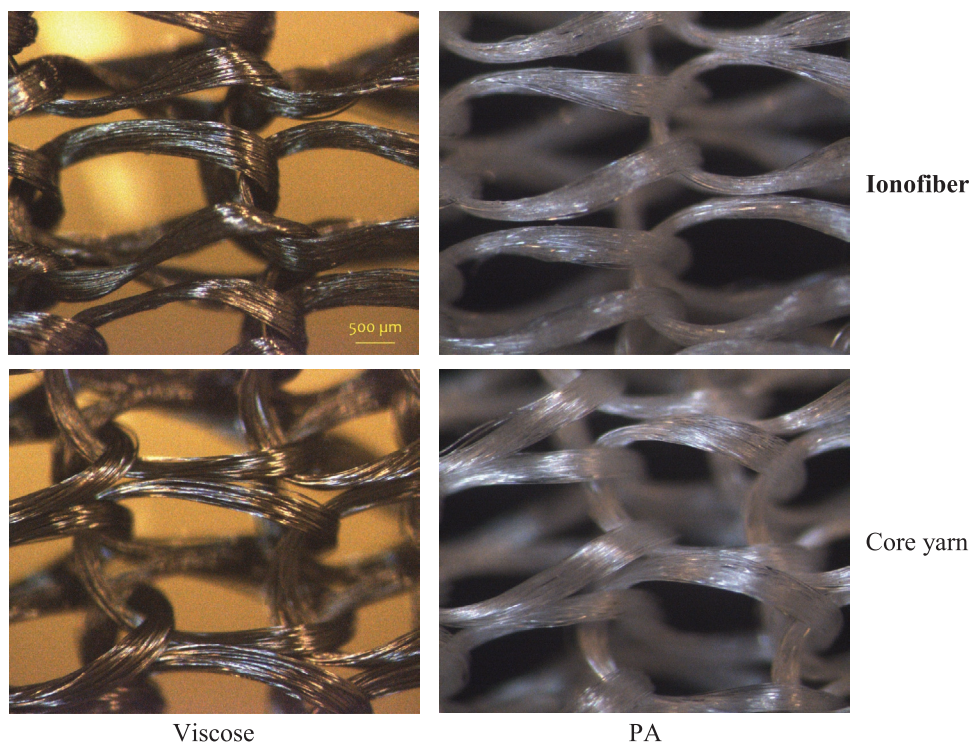

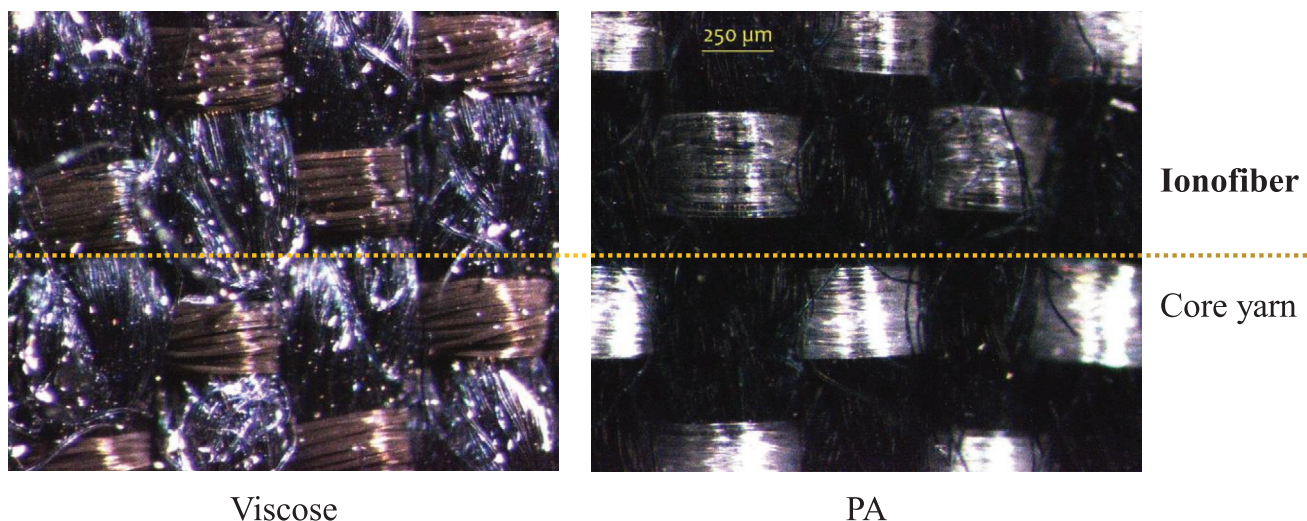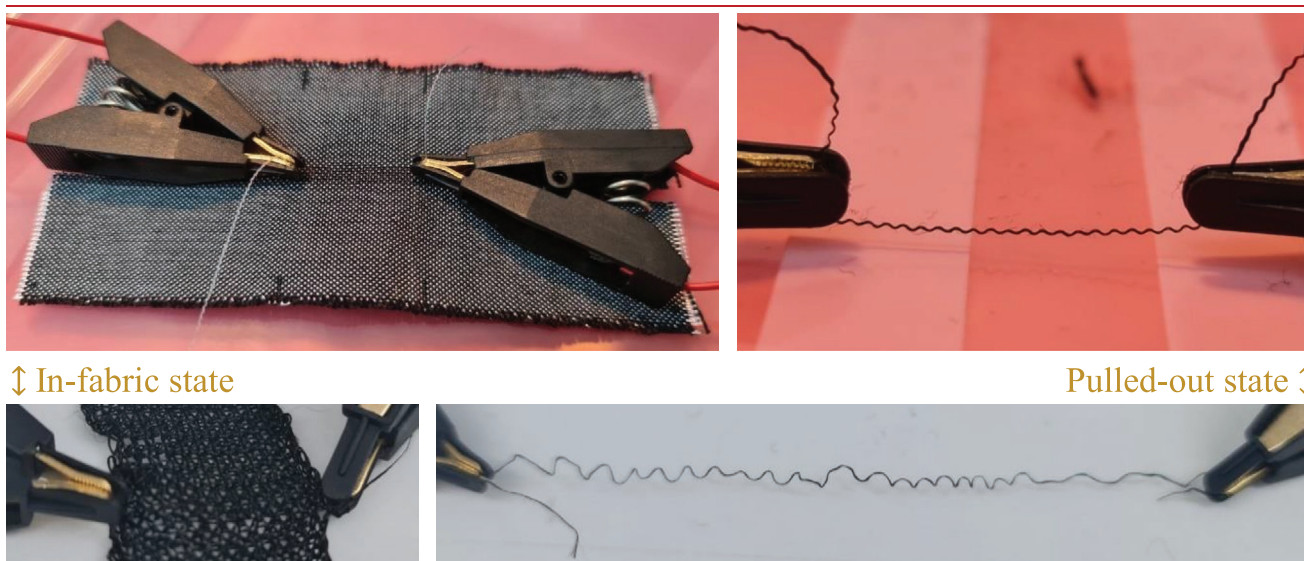**Figure 19.** Microscopy of the 15 rows knitted samples illuminated from above (shared scale bar).

**ADVANCED
SCIENCE NEWS**

www.advancedsciencenews.com

**ADVANCED
MATERIALS
TECHNOLOGIES**

www.advmattechnol.de

Figure 20. Microscopic pictures of the ionofibers versus core yarns inside the woven fabrics (shared scale bar).

2.7. Application Demonstration

To demonstrate that the ionofibers can be used for i-textile applications, the 15 rows knitted sample made with PA-TT25 was used as a strain and pressure i-textile sensor. The motivation behind this demonstration was to prove that the ionofibers are mechanoelectrical sensors able to translate a mechanical solicitation into low voltage signal according to principle of ionotronics.[32] For this demonstration, the i-textile sensor was fixed on a glove so that the ionofiber section of the sample was positioned on the back side of the index finger, right above the proximal interphalangeal joint, or middle joint (**Figure 24**). Thus, by extending, resting or flexing the index finger, the i-textile sensor experienced different levels of stretch and pressure.

These different levels of stretch and pressure should result in the variation of the electrical response respectively due to i) piezoresistivity, i.e., a change of resistance of the ionofibers as a function of elongation,[33] and ii) piezoionic effect, i.e., a variation of electrical signal as a function of pressure-induced redistribution of mobile ions in the gel.[34] A constant potential of 2 V was applied between the gold-plated electrodes fixed through the loops of the first and last row of the ionofiber section. The current signal was measured in the range of hundreds of nanoamperes. Any stretch or pressure on the i-textile sensor prompted a noticeable and substantial variation of the resulting current (**Figure 25**; Movie S5, Supporting Information). The variations amounted to roughly 25% of the current in resting position. A long press followed by a quick press was

Figure 21. Clamping of the ionofibers for the in-fabric and pulled-out states. Crimp measured: 15% for woven fibers and 600% for knitted fibers.

ADVANCED
SCIENCE NEWS
www.advancedsciencenews.com

ADVANCED
MATERIALS
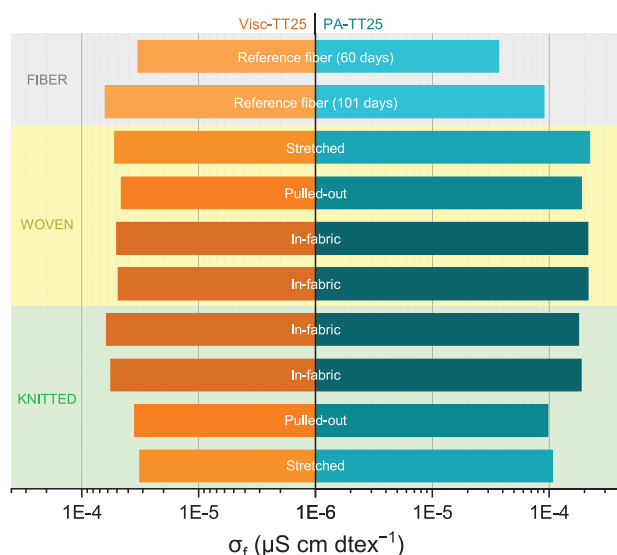TECHNOLOGIES
www.advmattechnol.de

Figure 22. Comparison of the fiber conductivity of an ionofiber before and after textile processing. Results are presented as single measured values, with two measurements on in-fabric ionofibers. All the measurements were done in the same ambient conditions, with the exception of the reference ionofibers 60 days after coating taken from Figure 15. Average ambient conditions: 22.6 °C and 46% RH.

sequentially done on the i-textile sensor in rest position. Each press resulted in a fast rise of the current until release.

This demonstration confirms the usability of the ionofibers in the context of low-voltage ionotronic applications. The ionic nature of the conductivity together with the conformal nature of these surface ionofibers can allow for many in-air applications in terms of electrochemistry. Therefore, ionofibers could lead to a new generation of i-textile and broaden the area of ionotronics.

3. Conclusion

In-air, ionically conductive fibers or ionofibers were produced by functionalizing commercial core yarns with a conductive ionogel coating. The ionogel coating also rendered the ionofibers more flexible and conformable than their core yarn counter parts. We showed that ionogels can be successfully coated on two categories of textile fibers, namely, synthetic fibers and cellulose fibers. Yet, coating the ionogel exhibited different levels of effect depending on the core yarn

Table 3. Comparison of the resistances per unit length of fabric (R/L) and the ratios between the multiple R/L proving interconnections within the knitted samples. The in-fabric R/L were calculated as the mean of the two measurements done on the single row knitted samples, whereas the R/L of both directions were measured on the 15 rows knitted samples. Results are presented as single measured/calculated values.

Knitted sample	In-fabric R/L [MΩ cm^{-1}]	Ratio ↔	15 rows course R/L [MΩ cm^{-1}]	Ratio ↔	15 rows wale R/L [MΩ cm^{-1}]
Visc-TT25	644	2.05	314	1.10	286
PA-TT25	223	6.41	34.8	5.28	6.58

used, emphasizing the importance of the selection of the core yarn. Indeed, results have shown that these ionofibers are to be regarded as composites. These ionofibers achieved their main function of conducting electric current in the range of 10^{-5} µS cm dtex^{-1} (analogous to 10^{-5} S cm^{-1}) at low ambient relative humidity (10% RH). Owing to the hygroscopic effect of EMIm OTf, a higher ambient relative humidity (around 45–50% RH) increased their fiber conductivity in the range of 10^{-4} µS cm dtex^{-1}. The ionofibers were shown to be homogeneous, regular and stable electrically as well as mechanically robust. The ionogel coating withstood the fabric manufacturing processes, which were knitting and weaving, at the pattern making level. The ionofibers that were seamlessly integrated into fabrics showed neither clear signs of visual nor functional degradation. Due to the improved flexibility of the ionofibers, the conformality of the fabrics was enhanced, offering promising prospects for ionotronics as to match biological interfaces. We showcased this by using the ionofibers as part of a knitted section of a fabric in an application demonstration. The strain and pressure i-textile sensor embodied the usability of ionofibers close to the skin in the context of low-voltage ionotronic applications.

Working toward an upscaled coating process, the possibility of producing continuously ionofibers via UV-curing would open up for the creation of addressable systems by advanced weaving and knitting patterns. This will eventually form a new generation of ionotronic devices.

4. Experimental Section

Chemicals: Trimethylolpropane tris(3-mercaptopropionate) (TT), poly(ethylene glycol) diacrylate (DA, average M_n of 700), and 1-ethyl-3-methylimidazolium trifluoromethanesulfonate (EMIm OTf) were supplied by Sigma-Aldrich (Germany). DT was supplied by TCI EUROPE N.V. (Belgium). All the reagents were used without further purification.

Preparation of ILsoln: Pure acetic acid (AcOH) was added into EMIm OTf then stirred to obtain an ionic liquid solution ILsoln of 2.5 wt% AcOH. After stirring, ILsoln was left in a closed vial for at least a day before use.

Preparation of the Ionogel Precursors: The ionogel precursor was obtained by carefully weighing and adding the different components in a vial according to the formulations in Table 1 in the following order: TT > DT > DA > ILsoln.

The precursors were then quickly stirred using a Vortex-Genie 2 vortex mixer from Scientific Industries, Inc. (USA) at a medium speed to prevent the formation of bubbles that would influence the quality of the coating.

Tensiometry: Tensiometry was performed using Attension Theta Optical Tensiometer from Biolin Scientific AB (Sweden/Finland) in pendant drop and meniscus modes. The liquid probes used for the evaluation of the surface energy of the core yarns were Milli-Q water and Diiodomethane (MI) supplied by Sigma-Aldrich (Germany). Their surface tensions, 72.8 and 50.8 mN m^{-1}, were taken from the literature.[24]

Extractible Content: The extractible content of the ionogel films was obtained by the loss of the mass between the ionogel films before and after extraction of the liquid part of the gels divided by the mass before extraction. The extraction was performed by soaking the ionogel in ethanol for 6 h before being dried in a vacuum oven at ambient temperature.

Optical Microscopy: Optical observation was performed using an SMZ800 stereo/photomicroscope equipped with a P-SXY64 XY Stage and a C-DSD230 Diascopic stand from Nikon (Japan) for the fiber
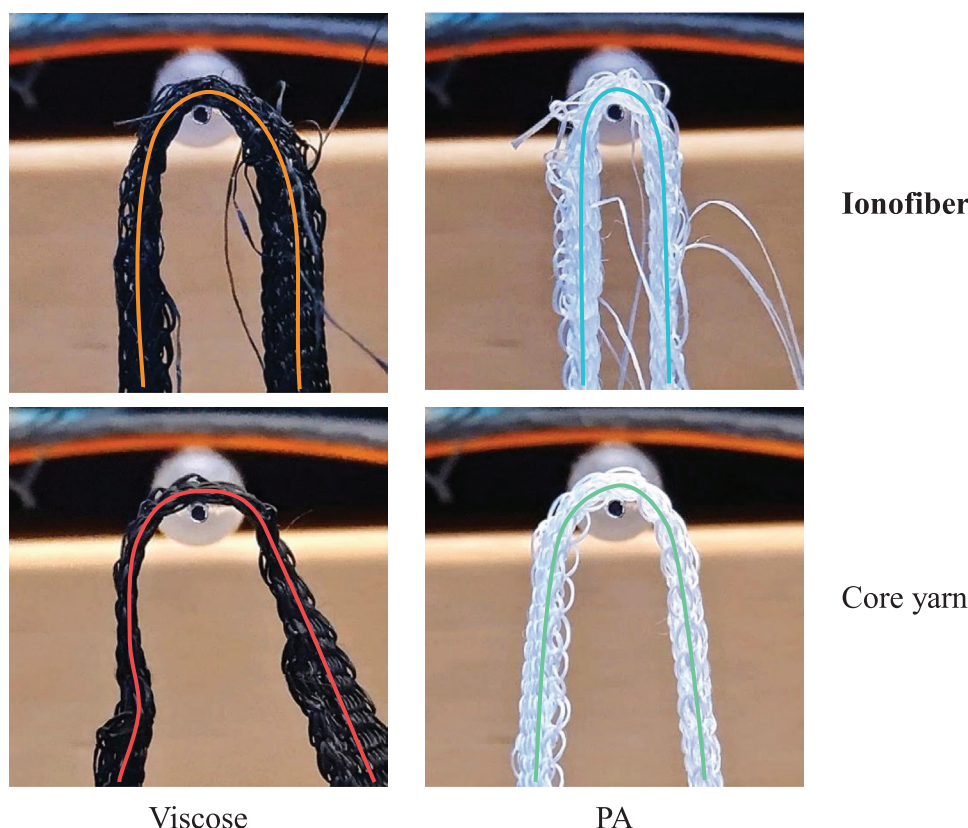
**ADVANCED
SCIENCE NEWS**

www.advancedsciencenews.com

**ADVANCED
MATERIALS
TECHNOLOGIES**

www.advmattechnol.de

Figure 23. Analysis of the curvature obtained by dropping on the tip of a pipette the 15 rows knitted samples versus knitted samples made from core yarns.

morphology along its length, whereas an M-100FL microscope from Optika SRL (Italy) was used for the cross-section morphology.

Fiber Conductivity: Conductivity tests were carried out on an Autolab PGSTAT204 potentiostat/galvanostat instrument with an FRA32M module from Metrohm (Switzerland). The excitation signal for the EIS was sine wave type of an amplitude of 0.5 V_{PK} around 0 V at in the frequency range of 100 kHz to 0.1 Hz with a step of 15 points per decade, an integration time of 15 s and 3 integration cycles.

Tensile Testing: Elastic behavior and ultimate properties of the samples were studied with a Mesdan (Italy) 2512A tensile tester in a conditioned room (21 °C and 65% RH). The tensile tests were performed using a pneumatic yarn clamp equipped with a cell of 0.1 kN (resolution: 1 cN), at the speed of 100% elongation min^{-1}. The data recording is done every 0.1 mm elongation. Samples were 50 mm long for ionofibers and

250 mm for core yarns. Tests were conducted five times for each core yarn and three times for each combination of ionogel and core yarn.

Dynamical Mechanical Thermal Analysis: Viscoelastic properties were studied using a Q800 dynamical mechanical–thermal analyzer from TA Instruments (USA). DMTA was performed in tensile mode to determine the storage modulus E', loss modulus E'' and loss factor tan δ. The samples were tested with a strain of 1% for PA, 0.1% for Visc, and 0.5% for the ionogel films at a frequency of 1 Hz and a pretension of 0.2 N using the film tension clamp provided by the manufacturer. A temperature sweep was also applied from −50 to 110 °C or up to degradation temperature with a ramp of 3 °C min^{-1}.

Statistical Analysis: Microsoft Excel was used for statistical analysis. The results are expressed as single measured/calculated values or mean values with CI (confidence interval based on the standard error of the
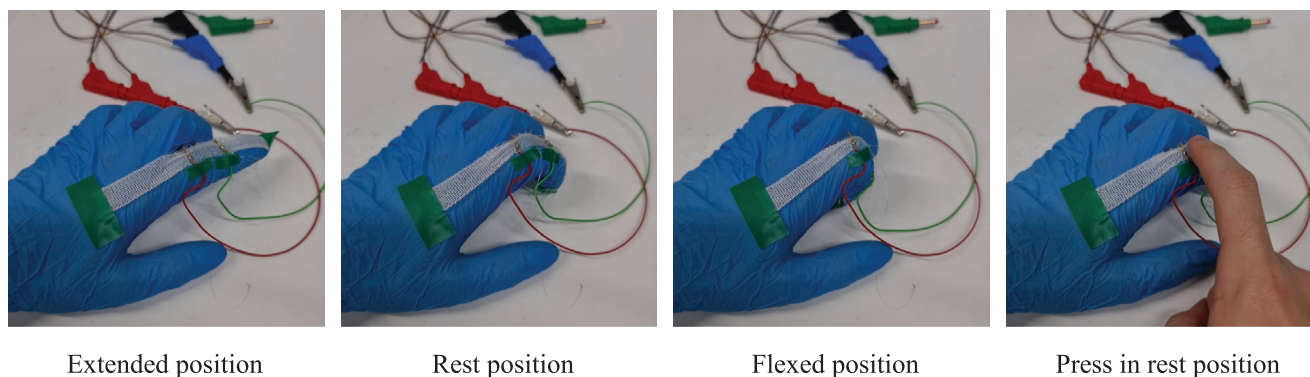

Figure 24. I-textile sensor and the different finger positions operated.
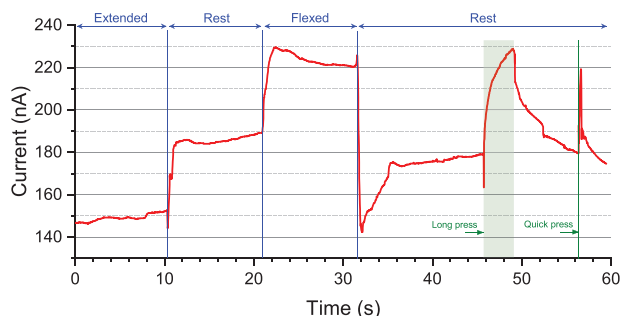
Figure 25. Current over time with a constant potential of 2 V, in respect of the electrochemical stability window of EMIm OTf (−1.8 to 2.3 V). The operated positions (in blue) are given as finger positions.

mean). Sample sizes are indicated for each experiment in the figure legend and additionally in the experimental section. Due to small sample sizes ($n < 30$), this resulted in limited statistical power for assessing significant differences.[35] Therefore, confidence intervals were provided for all the mean values calculated.

Supporting Information

Supporting Information is available from the Wiley Online Library or from the author.

Conflict of Interest

The authors declare no conflict of interest.

Data Availability Statement

The data that support the findings of this study are available from the corresponding author upon reasonable request.

[1] R. Sinclair, in *Textiles and Fashion*, Vol. *1* (Ed: R. Sinclair), Woodhead Publishing, Cambridge, UK **2015**, Ch. 1.

[2] a) K. Schischke, N. F. Nissen, M. Schneider-Ramelow, *MRS Commun.* **2020**, *10*, 69; b) E. Dauzon, X. Sallenave, C. Plesse, F. Goubard, A. Amassian, T. D. Anthopoulos, *Adv. Mater.* **2021**, *33*, 2101469.

[3] L. Guo, L. Sandsjö, M. Ortiz-Catalan, M. Skrifvars, *Text. Res. J.* **2020**, *90*, 227.

[4] H. Mattila, *Textiles and Fashion*, Vol. *1* (Ed: R. Sinclair), Woodhead Publishing, Cambridge, UK **2015**, Ch. 15.

[5] L. Guo, T. Bashir, E. Bresky, N.-K. Persson, *Smart Textiles and Their Applications*, Vol. *1* (Ed: V. Koncar), Woodhead Publishing, Duxford, UK **2016**, p. 657.

[6] T. Agcayazi, K. Chatterjee, A. Bozkurt, T. K. Ghosh, *Adv. Mater. Technol.* **2018**, *3*, 1700277.

[7] C. Yang, Z. Suo, *Nat. Rev. Mater.* **2018**, *3*, 125.

[8] a) A. Vioux, L. Viau, S. Volland, J. Le Bideau, *C. R. Chim.* **2010**, *13*, 242; b) J. Le Bideau, L. Viau, A. Vioux, *Chem. Soc. Rev.* **2011**, *40*, 907.

[9] D. R. MacFarlane, M. Kar, J. M. Pringle, *Fundamentals of Ionic Liquids*, Wiley-VCH, Weinheim, Germany **2017**, Ch. 1.

[10] E. Andrzejewska, A. Marcinkowska, A. Zgrzeba, *Polimery* **2017**, *62*, 344.

[11] C. H. Yang, B. Chen, J. J. Lu, J. H. Yang, J. Zhou, Y. M. Chen, Z. Suo, *Extreme Mech. Lett.* **2015**, *3*, 59.

[12] S. Y. Kim, E. Jee, J. S. Kim, D. H. Kim, *RSC Adv.* **2017**, *7*, 23820.

[13] C. Yang, S. Cheng, X. Yao, G. Nian, Q. Liu, Z. Suo, *Adv. Mater.* **2020**, *32*, 2005545.

[14] X. Shi, Y. Zuo, P. Zhai, J. Shen, Y. Yang, Z. Gao, M. Liao, J. Wu, J. Wang, X. Xu, Q. Tong, B. Zhang, B. Wang, X. Sun, L. Zhang, Q. Pei, D. Jin, P. Chen, H. Peng, *Nature* **2021**, *591*, 240.

[15] M. Yao, B. Wu, X. Feng, S. Sun, P. Wu, *Adv. Mater.* **2021**, *33*, 2103755.

[16] A. Abutaleb, D. Lolla, A. Aljuhani, H. U. Shin, J. W. Rajala, G. G. Chase, *Fibers* **2017**, *5*, 33.

[17] S. Rana, T. Carvalho, R. Fangueiro, P. Vidinha, *Polym. Adv. Technol.* **2013**, *24*, 191.

[18] L. Allison, S. Hoxie, T. L. Andrew, *Chem. Commun.* **2017**, *53*, 7182.

[19] P. K. Hari, in *Woven Textiles*, Vol. *1* (Ed: K. L. Gandhi), Woodhead Publishing, Cambridge, UK **2012**, Ch. 1.

[20] W. E. Morton, J. W. S. Hearle, in *Physical Properties of Textile Fibres*, 4th ed. (Eds: W. E. Morton, J. W. S. Hearle), Woodhead Publishing, Cambridge, UK **2008**.

[21] Y. Zhong, G. T.-M. Nguyen, C. Plesse, F. Vidal, E. W. H. Jager, *J. Mater. Chem. C* **2019**, *7*, 256.

[22] T. Young, *Philos. Trans. R. Soc.* **1804**, *95*, 65.

[23] A. Dupré, *Théorie mécanique de la Chaleur*, Gauthier-Villars, Paris, France **1869**.

[24] a) P.-S. d. Laplace, in *Traité de Mécanique Céleste*, Vol. *4*, Courcier, Paris, France **1805**; b) C. F. Gauss, *Principia Generalia Theoriae Figurae Fluidorum in Statu Aequilibrii*, Dieterichianis, Göttingen, Germany **1830**.

[25] F. M. Fowkes, *Ind. Eng. Chem.* **1964**, *56*, 40.

[26] J. Kloubek, *Adv. Colloid Interface Sci.* **1992**, *38*, 99.

[27] V. Raghavan, *Just Paint*, Golden Artist Colors, Inc, New Berlin, NY, USA **2014**.

[28] L. Kyllönen, A. Parviainen, S. Deb, M. Lawoko, M. Gorlov, I. Kilpeläinen, A. W. T. King, *Green Chem.* **2013**, *15*, 2374.

[29] a) J. Plateau, *Statique Expérimentale et Théorique des Liquides Soumis aux Seules Forces Moléculaires*, Gauthier-Villars, Paris, France **1873**; b) J. W. S. Rayleigh, *Philos. Mag.* **1892**, *34*, 145; c) D. Quéré, *Annu. Rev. Fluid Mech.* **1999**, *31*, 347.

[30] E. Karaca, F. Ozcelik, *J. Appl. Polym. Sci.* **2007**, *103*, 2615.

[31] H. Ota, K. Chen, Y. Lin, D. Kiriya, H. Shiraki, Z. Yu, T.-J. Ha, A. Javey, *Nat. Commun.* **2014**, *5*, 5032.

[32] G. Gu, H. Xu, S. Peng, L. Li, S. Chen, T. Lu, X. Guo, *Soft Rob.* **2019**, *6*, 368.

[33] a) K. Yang, G.-L. Song, L. Zhang, L.-W. Li, presented at *2009 Second Int. Conf. on Information and Computing Science*, Manchester, UK, May **2009**; b) G. Zhao, B. Lv, H. Wang, B. Yang, Z. Li, R. Junfang, G. Gui, W. Liu, S. Yang, L. Li, *Int. J. Smart Nano Mater.* **2021**, *12*, 307.

[34] a) P. G. d. Gennes, K. Okumura, M. Shahinpoor, K. J. Kim, *EPL* **2000**, *50*, 513; b) Y. Liu, Y. Hu, J. Zhao, G. Wu, X. Tao, W. Chen, *Small* **2016**, *12*, 5074.

[35] J. Leppink, K. Winston, P. O'sullivan, *Perspect. Med. Educ.* **2016**, *5*, 122.